JPE 15-1-22

http://dx.doi.org/10.6113/JPE.2015.15.1.235
ISSN(Print): 1598-2092 / ISSN(Online): 2093-4718

Reactive Current Assignment and Control for DFIG Based Wind Turbines during Grid Voltage Sag and Swell Conditions

Hailiang Xu†, Xiaojun Ma*, and Dan Sun**

†**Department of Control Engineering, Academy of Armored Force Engineering, Beijing, China
**College of Electrical Engineering, Zhejiang University, Hangzhou, China

Abstract

This paper proposes a reactive current assignment and control strategy for a doubly-fed induction generator (DFIG) based wind-turbine generation system under generic grid voltage sag or swell conditions. The system's active and reactive power constrains during grid faults are investigated with both the grid- and rotor-side convertors (GSC and RSC) maximum ampere limits considered. To meet the latest grid codes, especially the low- and high-voltage ride-through (LVRT and HVRT) requirements, an adaptive reactive current control scheme is investigated. In addition, a torque-oscillation suppression technique is designed to reduce the mechanism stress on turbine systems caused by intensive voltage variations. Simulation and experiment studies demonstrate the feasibility and effectiveness of the proposed control scheme to enhance the fault ride-through (FRT) capability of DFIG-based wind turbines during violent changes in grid voltage.

Key words: Convertor, Doubly Fed Induction Generator (DFIG), High Voltage Ride-Through (HVRT), Low Voltage Ride-Through (LVRT), Reactive current support

I. INTRODUCTION

Doubly fed induction generators (DFIGs) have been recognized as the most promising technology in wind energy conversion systems [1], [2]. When compared to other types of wind turbines (WTs), the DFIG-based turbines have some attractive advantages, such as small convertor capacity, relatively wide operation speed region, competitive durability and so on. However, DFIGs have also been found to be more vulnerable to grid disturbances, especially voltage sag and swell events. Since the number and capacity of WTs integrated into the electric networks is increasing, their dynamic behavior has become critical to the stability of power systems. As a result, modern grid codes have to stringently specify some voltage profiles, above which WTs must remain connected to the grid. This is commonly referred to as the low voltage ride-through (LVRT) requirement. In fact, the updated grid codes in Germany, Australia, UK, etc., even require WTs to withstand severe voltage swell conditions, which is usually referred to as the high voltage ride-through (HVRT) regulation [3]. Technically, LVRT and HVRT can be generally referred to as fault ride-through (FRT).

In terms of voltage sag scenarios, reported as the most common grid disturbance in industrial power systems, there have been many studies focusing on the electromagnetic transient process [4]-[7] and LVRT enhancement technologies [8]-[17] for DFIG-based WTs. The most commonly accepted technical solution applied in engineering can be summarized as follows: 1) for a mild voltage dip, only modified control strategies for grid-side and rotor-side converters (GSC and RSC) are applied, such as the flux demagnetizing approach [10]; 2) for a depth voltage drop, additional hardware devices, such as resistances connected in parallel with the RSC (the so called crowbar [11], [12]) or with the dc-link capacitor (the so called chopper [13]). On the one hand, they are equipped to suppress the inrush currents through the converters; on the other hand, the DFIG systems should be controlled to inject reactive current into the grid as soon as possible [3]. There are other solutions to protect convertors from destructive

Manuscript received Feb. 24, 2014; accepted Aug. 4, 2014
Recommended for publication by Associate Editor Seung-Ho Song.
†Corresponding Author: junzlh@126.com
Tel/Fax: +86-010-66717201, Academy of Armored Force Engineering
*Dept. of Control Eng., Academy of Armored Force Engineering, China
**College of Electrical Eng., Zhejiang University, China

over-currents, which enhances the uninterrupted operation ability of turbines. For example, static synchronous compensators (STATCOMs) [15], static var compensators (SVCs) [16] and dynamic voltage restorers (DVRs) [17], which have already been shown to be ideal auxiliary equipment to increase the FRT capability of a WT during grid voltage sag conditions.

However, in the case of voltage swells, the matters concerning the HVRT of DFIG-based WTs have not been so adequately explored in the literature. Voltage swell is a common grid anomaly and it usually emerges when the reactive power exceeds the needs in a power system. It was reported that 598 WTGs disconnected from the grid in Gansu Province, China, on February 24, 2011. Among these disconnections, 46% were caused by voltage sags and 54% were caused by voltage swells due to installed reactive compensators being unable to cut-off in time [18]. Consequently, in addition to LVRT, the HVRT behavior and its related technology for DFIG-based WTs need to be carefully considered and investigated. The transient process of DFIG-based WTs during voltage swells has been studied in [19]-[23]. A resonant controller, as a supplementary part of a traditional PI regulator, is introduced in [19] to improve the dynamic performance of current controller during voltage swell conditions. In [20] and [21], the application of hysteretic controllers are said to be more effective in improving the dynamic response of the system. Similarly, STATCOMs and DVRs have also been suggested as alternatives for the HVRT operation of WTs by compensating the line voltage back to its normal level [22], [23]. Obviously, this will significantly increase the hardware costs. In addition, the active and reactive power constraints during voltage swells have not been fully studied in the aforementioned studies. As a result, such proposed strategies are obviously unable to meet the strict grid code regulations.

For this reason, this paper proposes a reactive current assignment and comprehensive control approach for DFIG-based WT systems under grid voltage sag and swell conditions. The active and reactive power constrains of a system during grid faults are investigated while considering the maximum ampere limits of both the GSC and the RSC. To enhance its LVRT and HVRT capability, an adaptive reactive current control strategy is suggested with only traditional crowbar and dc-bus chopper protection-devices applied. In order to reduce the mechanism stress on the turbine shaft system caused by torque oscillations during grid voltage abnormalities, a torque-oscillation suppression technique is introduced. This paper is organized as follows. In Section II, the capability of the reactive current support for a DFIG system is analyzed. Section III then proposes a control scheme for both the GSC and RSC to meet grid codes during voltage sag or swell events. Simulation studies and experimental validations are presented in Sections IV and V, respectively. Finally, Section VI summarizes some valuable conclusions.

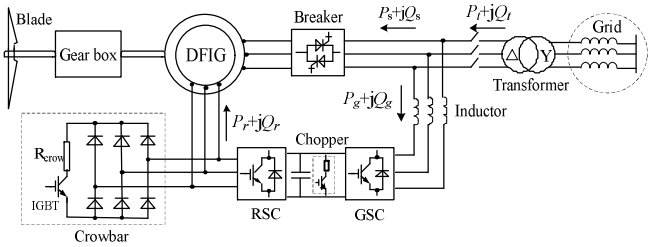

Fig. 1. The structure of a DFIG-based wind turbine.

II. Reactive Current Limit of a DFIG System

In order to put forward a control scheme capable of meeting the latest grid codes, it is necessary to evaluate the reactive power support capability for a DFIG system during grid voltage dip and swell conditions. As is well known, the active and reactive powers can be output from both the stator- and grid-sides of the DFIG system. In principle, the stator-side power of a DIFG is controlled by the RSC while the grid-side power is determined by the GSC. This means that the reactive power limitation of a DFIG-based WT is dominated by the capacity of the two converters.

The structure of a DFIG system with its power distribution (by motor convention) is shown in Fig. 1. From this the following power equations can be formulated:

$$\begin{cases} P_t = P_s + P_g \\ Q_t = Q_s + Q_g \end{cases} \tag{1}$$

where P_t, P_s and P_g represent the active powers of the overall system, the stator-side and the grid-side, respectively, with Q_t, Q_s and Q_g being their corresponding reactive powers.

Furthermore, if the copper and core losses of the DFIG windings are ignored, the stator- and grid-side active powers can be expressed in terms of the total active power and the slip ratio, i.e.:

$$\begin{cases} P_s = \dfrac{P_t}{1-s} \\ P_g = -\dfrac{sP_t}{1-s} \end{cases} \tag{2}$$

where $s = (\omega_s - \omega_r)/\omega_s$ is the slip ratio.

Based on the above power equations, the reactive current limitations for the GSC and RSC can be deduced. The voltage swell case will be paid more attention since the sag case has been discussed more often in the literature [8]-[17].

A. Current Limit of the GSC

The stability of the dc-bus voltage is the premise of the uninterruptible operation for DFIG systems during grid voltage disturbances. Thus, the reactive and active current constrains of the GSC will be studied in this section.

The steady-state voltage equation of the GSC in the

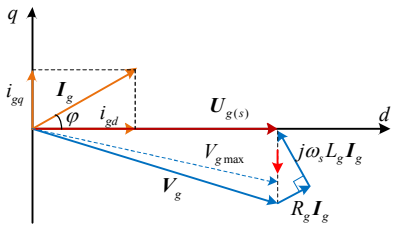

Fig. 2. The spatial relationship of GSC steady voltage vectors.

synchronously rotating coordinate can be expressed as:

$$\begin{cases} U_{gd} = R_g I_{gd} - \omega_s L_g I_{gq} + V_{gd} \\ U_{gq} = R_g I_{gq} + \omega_s L_g I_{gd} + V_{gq} \end{cases} \tag{3}$$

where U_{gd} and U_{gq} are the d- and q-axis grid voltages. I_{gd} and I_{gq} are the d- and q-axis grid currents. L_g and R_g are the input inductance and resistance of the GSC, respectively.

Meanwhile, the dc-bus voltage should obey the following power balance relationship, i.e.:

$$CV_{dc}\frac{dV_{dc}}{dt} = P_g - P_r. \tag{4}$$

According to Eq. (3), the steady-state voltage space vector diagram of the GSC can be depicted as in Fig. 2, with φ being the power factor angle. From Fig. 2, it can be concluded that the terminal of the output voltage vector V_g should always fall on the hypotenuse of the impedance triangle with its magnitude restricted by the rated operational voltage across the dc-bus capacitor. This is actually based on the voltage space vector modulation theory, which states that without over-modulation the modulation ratio m needs to meet the following equation:

$$m = \sqrt{V_{gd}^2 + V_{gq}^2} \,/\, (V_{dc}/2) \le 2/\sqrt{3}. \tag{5}$$

If grid voltage orientation (SVO) is adopted, U_{gd}=U_g and U_{gq}=0, where U_g is the magnitude of the grid phase voltage vector and is equal to U_s according to Fig. 1. Meanwhile, if the small voltage drop across R_g is ignored, Eq. (3) can be further simplified as:

$$\begin{cases} V_{gd} = U_g + \omega_s L_g I_{gq} \\ V_{gq} = -\omega_s L_g I_{gd} \end{cases}. \tag{6}$$

Substituting (6) into (5), it can be derived that:

$$V_{dc} \ge \sqrt{3}\sqrt{\left(U_g + \omega_s L_g I_{gq}\right)^2 + \left(-\omega_s L_g I_{gd}\right)^2}. \tag{7}$$

Equation (7) gives the operation constrains of the GSC with the dc-bus voltage, grid voltage, inductor and load currents being the main parameters. It can be found that the minimum value of the dc-bus voltage should be no less than the grid line voltage, i.e., $V_{dc} \ge \sqrt{3}U_g$ when the GSC is operated in unity power factor (UPF) mode, i.e., I_{gq}=0. Actually, this is caused by the natural attribute of the GSC boost circuit. Based on the above discussion, the GSC reactive current limit can then be analyzed and acquired for

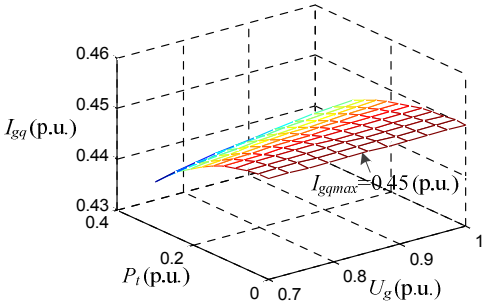

Fig. 3. The curves of GSC reactive current vs. the total active power and grid voltage.

voltage sags and swells.

1) Voltage Sag: For convenient analysis, a 3MW DFIG system is taken as an example with the parameters shown in TABLE I of the Appendix. The rated line voltage of the DFIG is 690V, while the normal dc-bus voltage is set to 1050V. When a voltage sag fault occurs, U_g will be brought down. Thus, Eq. (7) is easy to satisfy if the currents flowing through the GSC are not beyond the maximum ampere limit. In this case, the maximum reactive current output from the grid-side can be calculated as:

$$I_{gq} = \sqrt{\left(I_{g\max}\right)^2 - \left(I_{gd}\right)^2} = \sqrt{\left(I_{g\max}\right)^2 - \left(\frac{sP_t}{U_g(1-s)}\right)^2} \tag{8}$$

where I_{gmax} is the maximum ampere limit of the GSC and equal to 0.45p.u. in the example.

According to Eq. (8), it is obvious that the reactive power supporting capability of the GSC is determined by both the overall active power of the system and the slip ratio for a given maximum ampere limit. Fig. 3 shows the curves of the reactive current vs. the total active power and grid voltage for a given maximum generator speed, i.e., s= –0.3p.u. From this, it can be observed that the maximum reactive current is around 0.45p.u. when the total active power is set to zero.

2) Voltage Swell: It is worth pointing out that although the reactive current injection is helpful for the voltage recovery of a faulty power system, it is not the premise to satisfy the operation principle of the boost circuit for the GSC during voltage sags. In other words, the GSC reactive current can be set to zero under this circumstance if the reactive current required by the grid codes can be adequately provided through the stator-side of a DFIG system. However, this assignment is no longer valid for the voltage swell case. For example, if the GSC continues to operate in the UPF mode, the dc-bus voltage has to be increased to more than 1296V when the PCC voltage swells to 1.3p.u., which goes far beyond the rated operational voltage of dc-bus capacitor, i.e., 1050V. Thankfully, the GSC reactive current usually possesses an inductive property, which is useful for reducing the required dc-bus voltage.

According to Eq. (7), the required minimum reactive

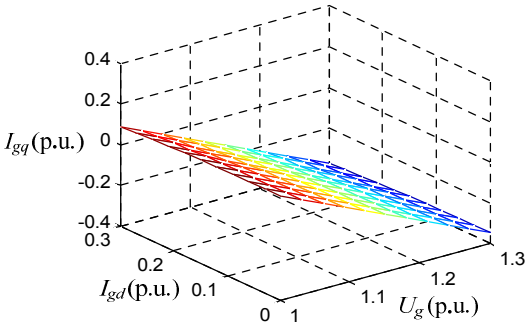

Fig. 4. The curves of the GSC reactive current vs. its active one and grid voltage.

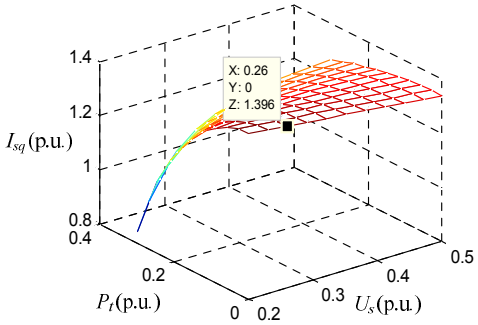

Fig. 5. The curves of stator reactive current vs. the total active power and grid voltage.

current during a voltage sag can be calculated as:

$$I_{gq\min}=\frac{1}{\omega_s L_g}\left(\sqrt{V_{dc}^2/3-\left(-\omega_s L_g I_{gd}\right)^2}-U_g\right), \tag{9}$$

which clearly indicates that the minimum reactive current depends on both the grid voltage (U_g) and the active current (I_{gd}) of the GSC, as illustrated in Fig. 4.

Meanwhile, it can be found from Fig. 4 that the minimum reactive current is mainly determined by the grid voltage. It is scarcely influenced by the active power. Hence, Eq. (9) can be further simplified as:

$$I_{gq\min}=\frac{1}{\omega_s L_g}\left(V_{dc}/\sqrt{3}-U_g\right). \tag{10}$$

Eq. (10) presents the minimum reactive current constrained by the natural attribute of the boost circuit.

Once the minimum reactive current is obtained, the active current of the GSC can be restricted by:

$$\left|I_{gd}\right|\le\sqrt{I_{g\max}^2-I_{gq}^2}. \tag{11}$$

As a result, the output minimum reactive power and the maximum active power can be integrated as:

$$\begin{cases}Q_{g\min}=-\dfrac{U_g}{\omega_s L_g}\left(V_{dc}/\sqrt{3}-U_g\right)\\ P_{g\max}=U_g\sqrt{I_{g\max}^2-I_{gq}^2}\times Sgn(s)\end{cases} \tag{12}$$

where:

$$Sgn(s)=\begin{cases}1, & s>0\\ 0, & s=0.\\ -1, & s<0\end{cases} \tag{13}$$

B. Current Limit of the RSC

The stator active and reactive powers of the DFIG can be expressed as [19]:

$$\begin{cases}P_s=-\dfrac{L_m}{L_s}U_s I_{rd}\\ Q_s=\dfrac{U_s}{\omega_s L_s}\left(U_s+\omega_s L_m I_{rq}\right)\end{cases}. \tag{14}$$

From Eq.(14), the magnitude of the rotor current can then be calculated as:

$$\begin{aligned}I_r&=\sqrt{I_{rd}^2+I_{rq}^2}\\ &=\sqrt{\left(\frac{L_s P_s}{L_m U_s}\right)^2+\left(\frac{L_s I_{sq}}{L_m}+\frac{U_s}{\omega_s L_m}\right)^2}.\end{aligned} \tag{15}$$

Consequently, by substituting (2) into (15), the stator-side reactive current I_{sq} can be obtained as:

$$I_{sq}=\sqrt{\left(\frac{L_m}{L_s}I_{r\max}\right)^2-\left(\frac{P_t}{U_s(1-s)}\right)^2}-\frac{U_s}{\omega_s L_s}. \tag{16}$$

Likewise, from Eq. (16) it can be found that once the maximum rotor current is determined, the output stator reactive current mainly depends on the total active power, the slip radio and the terminal voltage. Fig. 5 thus graphically shows the relationship of the stator reactive current vs. the total active power and grid voltage during a voltage sag at the maximum generator speed, i.e., s= –0.3p.u., with the maximum rotor current being 1.5p.u. (referred to the stator). By this curve, the maximum stator reactive current for a given stator voltage can be easily determined. For example, the calculated I_{sq} could reach up to 1.396p.u. (capacitive) for a grid voltage dip down to 26% of the rated value, with the total active power being equal to zero. Meanwhile, the maximum stator reactive current during voltage swell conditions can be obtained similarly from Eq. (16), but with the opposite polarity.

III. Proposed Control Scheme

A. Current Assignment

In the previous section, the maximum reactive currents of both the grid- and stator-sides of a DFIG system under voltage sag and swell conditions have been discussed in detail. In order to meet the grid codes, the reactive current references of the GSC and RSC will be preferentially assigned in this section. Moreover, the active current references of the two convertors will also be designed properly so as to maintain system stability. For the sake of convenience, the reactive power support requirement enforced by the German Grid Code is selected here as the

standard to be discussed.

1) Voltage Sag: According to the German Grid Code, WTs are required to provide capacitive reactive current as:

$$I_Q = \begin{cases} 2\times(1-U_s)I_N, & U_s \in [0.5p.u.,\ 0.9p.u.] \\ I_N, & U_s \in [0p.u.,\ 0.5p.u.) \end{cases} \tag{17}$$

where I_Q is defined as the required reactive current, and I_N is the rated current of the system, which is assumed to be 1.3p.u. in this paper.

Assume the maximum continuous currents of the GSC and RSC, i.e., $I_{g\max}$ and $I_{r\max}$ to be 0.45p.u. (the rated value is defined as 0.3p.u.) and 1.5p.u. (the stator and the rated value are defined as 1p.u.), respectively. Thus, according to Eq. (16), the maximum stator reactive power can then be calculated approximately as:

$$I_{sq\max} = L_m / L_s \times I_{r\max} \approx 1.41p.u. \tag{18}$$

Obviously, the reactive current required by the grid code can be adequately provided by the stator-side of the DFIG. Then the reactive current reference of the RSC can be set as:

$$I_{rq}^* = \begin{cases} \dfrac{2L_s}{L_m}(1-U_s)I_N, & U_s \in [0.5p.u.,\ 0.9p.u.] \\ \dfrac{L_s}{L_m}I_N, & U_s \in [0p.u.,\ 0.5p.u.) \end{cases} \tag{19}$$

It is worth noting that if the reactive current of the RSC is not beyond its limit, the active power should be controlled to restrain the generator speed upsurge. Accordingly, the RSC active current can be assigned as:

$$I_{rd}^* = \min\left\{-\frac{L_s P_s}{L_m U_s}, \sqrt{I_{r\max}^2 - I_{rq}^{*2}}\right\}. \tag{20}$$

Since the reactive current on this condition is entirely provided by the RSC, the GSC can be consequently controlled in the UPF state, i.e., $I_{gq}^* = 0$, with I_{gd}^* being the PI output of its voltage loop.

2) Voltage swell [25]: Similarly, during grid voltage swell conditions, WTs are required to inject current into the power system with the same intensity as for the voltage sag case, but of inductive property. As a result, the total required reactive current can be expressed as:

$$I_Q = 2\times(1-U_s)I_N,\ U_s \in [1.1p.u.,\ 1.3p.u.]. \tag{21}$$

Considering that the GSC has to inject a certain inductive current to ensure the safe operation of the capacitor, the reactive current required can be preferentially provided by the GSC. Fig. 6 illustrates the current-voltage curves obtained from Eqs. (10) and (21), from which it can be seen that the magnitude of the reactive current required by the inherent operation principle of the boost circuit is smaller than that required by the grid code. Hence, the partial required reactive current, marked by the slashed area in Fig. 6, should be supplemented by the stator-side of the DFIG.

As a result, the GSC output reactive current can be

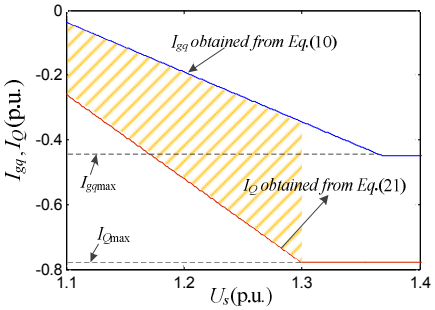

Fig. 6. Current-voltage curves obtained from Eqs. (10) and (21).

assigned as:

$$I_{gq}^* = \frac{1}{\omega_s L_g}\left(V_{dc}/\sqrt{3} - U_s\right) \tag{22}$$

with its maximum active current limited by:

$$I_{gd\max}^* = \sqrt{I_{g\max}^2 - I_{gq}^{*2}}. \tag{23}$$

As far as the RSC is concerned, the output stator reactive current can be determined as:

$$I_{sq}^* = \left[2\times(1-U_s)I_N - I_{gq}^*\right]. \tag{24}$$

Consequently, the RSC reactive current should be computed as follows:

$$\begin{aligned} I_{rq}^* &= -\frac{L_s I_{sq}^*}{L_m} - \frac{U_s}{\omega_s L_m} \\ &= \frac{L_s}{L_m}\left[2\times(U_s-1)I_N + I_{gq}^*\right] - \frac{U_s}{\omega_s L_m}. \end{aligned} \tag{25}$$

According to Fig. 1, if the copper loss of the generator windings is ignored, the relationship between the grid- and stator-side powers of the DFIG system can be simplified as:

$$P_g = P_r \approx -sP_s \tag{26}$$

where P_r is the output active power of the RSC.

Due to the fact that the current capacity of the RSC is usually designed a littler larger than that of the GSC, the output active power of the RSC during the voltage swell cases should be set so that it is not more than that of the GSC. Thus, according to Eqs. (14) and (26), the maximum active current of the RSC can be constrained as:

$$I_{rd\max} = \frac{P_{g\max} L_s}{sU_s L_m}. \tag{27}$$

Meanwhile, if the current limit of the RSC is considered, the maximum active current reference of the RSC can be further limited by:

$$I_{rd\max}^* = \min\left\{\frac{P_{g\max} L_s}{sU_s L_m}, \sqrt{I_{r\max}^2 - I_{rq}^{*2}}\right\}. \tag{28}$$

B. Current Controller Design

Once the reactive and active current references are acquired as requested by the grid regulations, a precise current controller must be properly designed to regulate them accurately and rapidly. Since it is capable of gaining zero

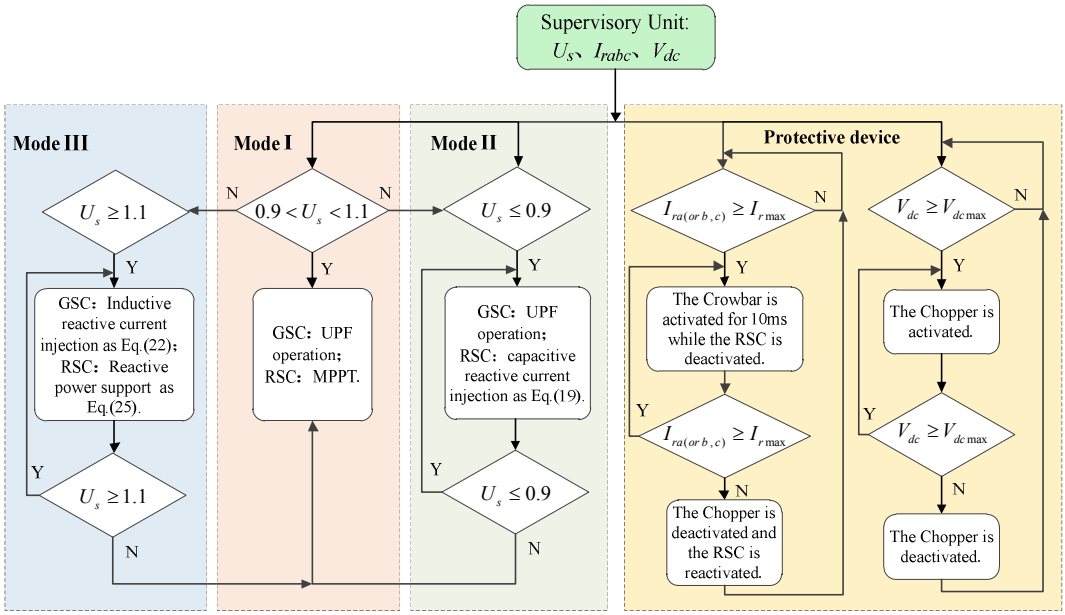

Fig. 7. The schematic diagram of the proposed control scheme.

steady-state error for the dc components, the traditional PI controller is usually applied in the vector control of distributed power generation systems. However, due to its limited bandwidth, the PI controller is not able to achieve a very effective response to the ac components, which usually occur during voltage sag or swell scenarios [11], [23]. It is well-known that without a proper control design, the ac components in the currents will lead to destructive oscillations in the electromagnetic torque for DFIG-based WTs [24]. As a result, they should be inhibited to the greatest extent possible. Thus, a torque-oscillation suppression approach needs to be investigated, which can be commenced from setting the auxiliary current references.

In the synchronously rotating reference frame, the stator flux vector of the DFIG can be expressed as:

$$\boldsymbol{\psi}_{sdq} = L_s \boldsymbol{I}_{sdq} + L_m \boldsymbol{I}_{rdq}. \tag{29}$$

Consequently, there is:

$$\boldsymbol{I}_{sdq} = \left(\boldsymbol{\psi}_{sdq} - L_m \boldsymbol{I}_{rdq}\right) / L_s. \tag{30}$$

Meanwhile, the stator voltage vector can be calculated by the stator flux vector as:

$$\begin{aligned} \boldsymbol{U}_{sdq} &\approx d\left(\boldsymbol{\psi}_{sdq+} + \boldsymbol{\psi}_{sdq0} e^{-j\omega_s t}\right)/dt + j\omega_s\left(\boldsymbol{\psi}_{sdq+} + \boldsymbol{\psi}_{sdq0} e^{-j\omega_s t}\right) \\ &= j\omega_s \boldsymbol{\psi}_{sdq+} \end{aligned} \tag{31}$$

where the subscripts "+" and "0" represent the respective positive- and dc-sequence components.

In this manner, the electromagnetic power can be calculated as:

$$\begin{aligned} P_e &= \mathrm{Re}\left[j\omega_s \boldsymbol{\psi}_{sdq} \times \hat{\boldsymbol{I}}_{sdq} + j(\omega_s - \omega_r)\boldsymbol{\psi}_{rdq} \times \hat{\boldsymbol{I}}_{rdq} \right] \\ &= \omega_r L_m / L_s \times \mathrm{Im}(\boldsymbol{\psi}_{sdq} \times \hat{\boldsymbol{I}}_{rdq}) \\ &= P_{edc} + P_{e\cos}\cos(\omega_s t) + P_{e\sin}\sin(\omega_s t) \end{aligned} \tag{32}$$

where:

$$\begin{bmatrix} P_{edc} \\ P_{e\cos} \\ P_{e\sin} \end{bmatrix} = \frac{L_m \omega_r}{L_s} \begin{bmatrix} \psi_{sq+} & -\psi_{sd+} & \psi_{sq0} & -\psi_{sd0} \\ \psi_{sq0} & -\psi_{sd0} & \psi_{sq+} & -\psi_{sd+} \\ -\psi_{sd0} & -\psi_{sq0} & \psi_{sd+} & \psi_{sq+} \end{bmatrix} \begin{bmatrix} I_{rd}^* \\ I_{rq}^* \\ I_{rd0}^* \\ I_{rq0}^* \end{bmatrix}. \tag{33}$$

As a result, the auxiliary dc current references of I_{rd0}^* and I_{rq0}^* can be acquired by setting $P_{e\cos} = 0$ and $P_{e\sin} = 0$ in Eq. (30):

$$\begin{cases} I_{rd0}^* = \dfrac{\psi_{sq0} I_{rd}^* - \psi_{sd0} I_{rq}^*}{\psi_{s+}} \\ I_{rq0}^* = -\dfrac{\psi_{sd0} I_{rd}^* + \psi_{sq0} I_{rq}^*}{\psi_{s+}} \end{cases}. \tag{34}$$

To simultaneously regulate both the dc and ac components, a compound of a PI regulator plus a resonant controller (PI-R) is introduced here with its transfer function being:

$$C_{\mathrm{PI-R}}(s) = K_p + \frac{K_i}{s} + \frac{2K_r \omega_c s}{s^2 + 2\omega_c s + \omega_s^2}. \tag{35}$$

where K_p, K_i and K_r are the proportional, integral and resonant parameters, respectively, and with ω_c being the cutoff frequency, introduced into the resonant part of the controller to reduce its sensitivity to slight frequency variations at the resonant pole [26]. It is worth noting that the proposed PI-R controller is insensitive to parameter variations, which has been demonstrated in [27], [28]. Since the resonant controller is tuned at the synchronous frequency, the PI-R can nullify the errors of the dc components as well as the ac components at the frequency of ω_s.

C. Control Logic

Once the reactive current control strategy for DFIG based wind-turbine systems under generic grid voltage sag and swell conditions is founded, the concrete control logic to

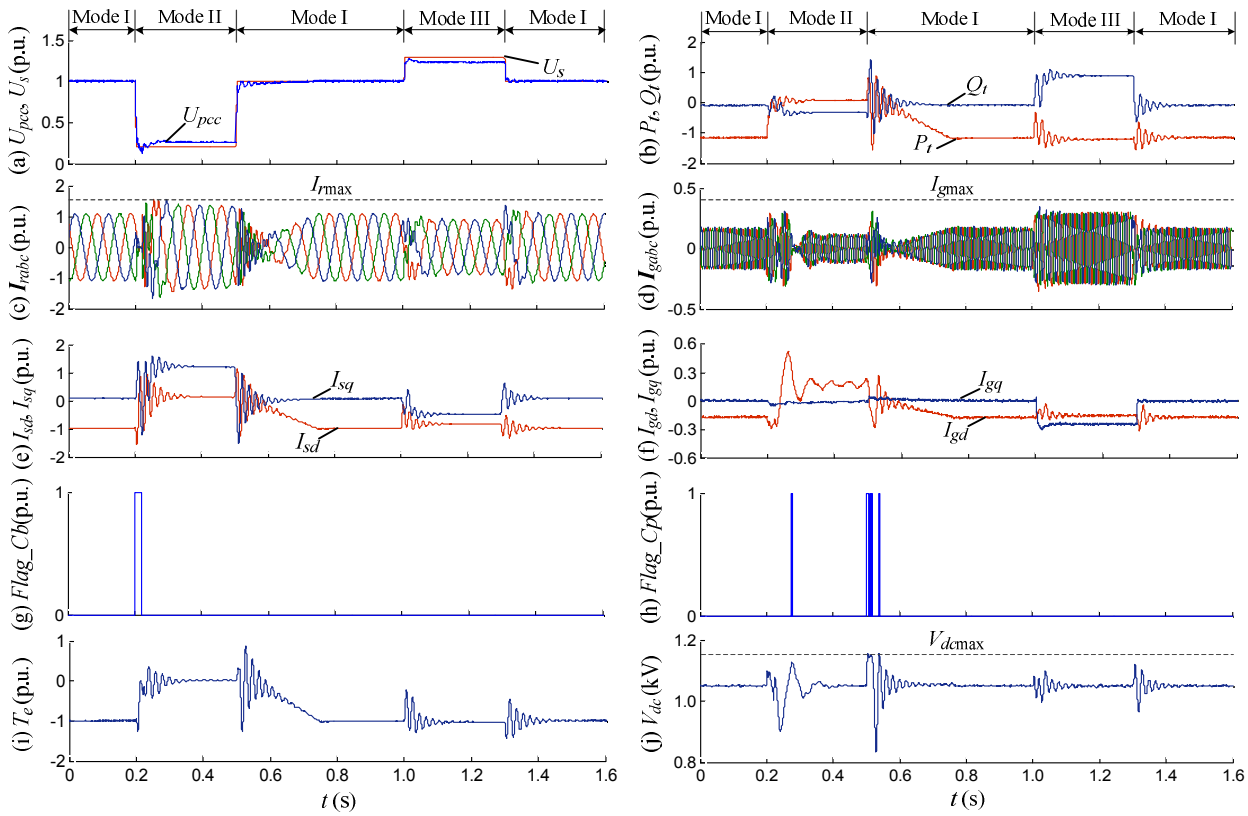

Fig. 8. Simulated results of the DFIG system with different operation modes under voltage sag and swell transients.

implement the proposed scheme seems to be predominant, and a schematic diagram of it is shown in Fig. 7. It is clear that the control scheme is designed with three operation modes: 1) mode I: maximum power point tracing (MPPT) mode [29], where the active and reactive current references of the GSC and RSC are assigned so that the system operates approximately in UPF; 2) mode II: LVRT operation; and 3) mode III: HVRT operation, where the fundamental active and reactive current references of the two convertors are given respectively as in part A of section III, with their auxiliary current references set as in part B of the same section. Furthermore, the reactive and active current references are momentarily changed to proper values with their corresponding modes according to the grid voltage U_s. Additionally, a group of protective devices, consisting of a traditional crowbar and a dc-bus chopper, are also equipped to suppress the inrush rotor currents if necessary (judged by I_{rabc} and V_{dc}).

IV. Simulation Studies

To validate the feasibility and effectiveness of the proposed control strategies, simulation studies were conducted with Matlab/Simulink. The simulated DFIG is rated at 3MW. Its parameters are listed in TABLE I and the system schematic diagram is shown in Fig. 1. The switching frequencies for both the RSC and GSC are 3kHz with the sampling frequencies set as 10kHz. Considering that the mechanical time constant is much larger than the electromagnetic one, the rotor speed is conditionally assumed to be fixed at 1.2p.u. in the simulation. In addition, a programmable ac source module was employed to emulate an irregular grid. Fig. 8 shows the simulated results for both the voltage sag and swell cases, with the three different control modes adopted and compared.

As can be seen in Fig. 8, under Mode I, where the grid voltage is 1p.u. (Fig. 8(a)), the total active and reactive powers of the system are 1.15p.u. and 0.08p.u. (capacitive), respectively (Fig. 8(b)). This means that the system was operated approximately at unity power factor. However, when a voltage dip fault is detected, the system's control mode switches immediately to Mode II. According to the grid code, the DFIG system needs to output 1.3p.u. of capacitive reactive current into the power network. This can be entirely provided by the DFIG stator-side, as shown as I_{sq} in Fig. 8(e). Consequently, the DFIG active current I_{sd} should set to be zero due to the limited current capacity of the RSC, while the GSC is operated nearly in the UPF state, as displayed in Fig. 8(f). Meanwhile, the crowbar and chopper (indicated in Figs. 8(g) and 8(h), with "1" denoting "activated") are activated respectively for tens of milliseconds according to the detected rotor currents and dc-bus voltage (as shown in Figs. 8(c) and

TABLE I
THE REQUIRED AND OUTPUTTED REACTIVE CURRENTS WITH DIFFERENT CONTROL MODES

Reactive currents	Mode I	Mode II	Mode III
I_{gq} (p.u.)	0	0	-0.26
I_{sq} (p.u.)	0.08	1.29	-0.50
I_{tq} (p.u.)	**0.08**	**1.29**	**-0.76**
I_Q (p.u.)	**0**	**1.3**	**-0.78**

(j)). Thanks to the optimization current assignment and valid controller design, the system is able to keep uninterruptable operation during such grid faults and inject the required current into the grid, which naturally meets the requirements of the grid code. Once the grid fault is cleared, the system's operation switches mildly from Mode II to Mode I with its active current setting gradually returning to its normal value in order to reduce the torque strike, as shown in Fig. 8(i).

Similarly, when a voltage swell fault occurs, the system's control mode switches quickly to Mode III, where the inductive reactive current is provided by both the GSC and RSC, with the former in priority. Unlike the voltage dip case, the final active power in the voltage swell case almost equals its normal value, as shown in Fig. 8(b). Although the GSC currents become much bigger than its normal value in this case, they are still lower than its maximum, as seen in Fig. 8(d).

Table I summarizes the reactive currents required by the grid code and output from the GSC and stator of the DFIG. It can be seen that the total output reactive current is a little smaller than that required since the stator voltage has been compensated to a relatively higher or lower level during grid faults, as shown in Fig. 8(a). After all, the reactive current requirement is well satisfied.

To thoroughly understand the importance of the reactive current assignment during a voltage swell, Fig. 9 illustrates the simulated results of the same DFIG system with null reactive current injection. It is obvious that although the chopper is effectively activated for a long time, the dc-bus voltage still rises to an unacceptable value due to the boost circuit characteristics of the GSC. As a result, it is essential to inject a certain reactive current into the grid by the GSC during a voltage swell. This is equally valuable for grid recovery.

Furthermore, simulation tests were conducted with a traditional PI controller to evaluate the effectiveness of the torque-oscillation suppression scheme, as shown in Fig.10. When compared to the corresponding waveforms in the same duration in Fig. 8, it is obvious that proposed method is valid for eliminating the destructive pulsations in electromagnetic torque. In addition, the scheme can also be used to suppress ripples in the dc-bus voltage and to reduce over-current in the GSC.

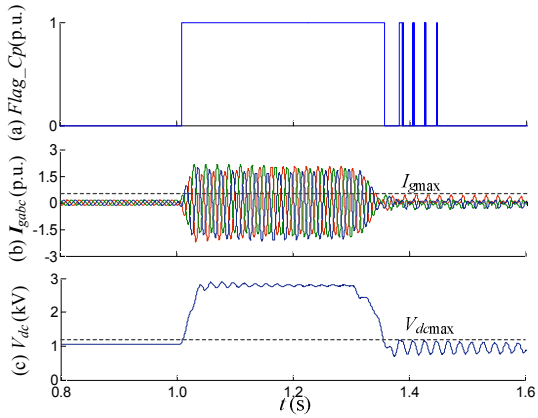

Fig. 9. Simulated results of the GSC with UPF operation during voltage swell condition.

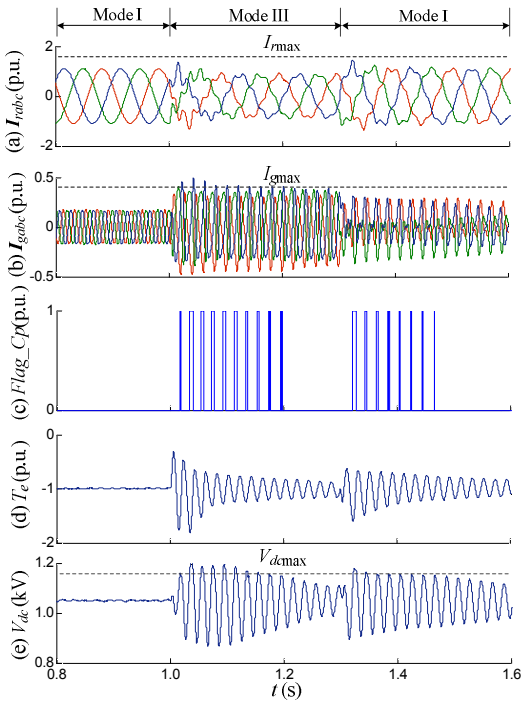

Fig. 10. Simulated results for the DFIG system with a traditional PI current controller during voltage swell conditions.

V. EXPERIMENT VALIDATIONS

In order to evaluate the feasibility and validity of the proposed control strategy in practice, experimental tests were carried out on a 5.5kW DFIG setup, the parameters of which are listed in TABLE II of the Appendix. The RSC and GSC are controlled by two TI TMS320F2812 DSPs and the switching frequencies for both converters are set at 2.5kHz with a sampling frequency of 10kHz.

Figs.11 (A) and (B) display the measured waveforms of the tested DFIG system during grid voltage sag and swell scenarios, respectively, with grid faults lasting for 300ms. The average output stator active and reactive powers during

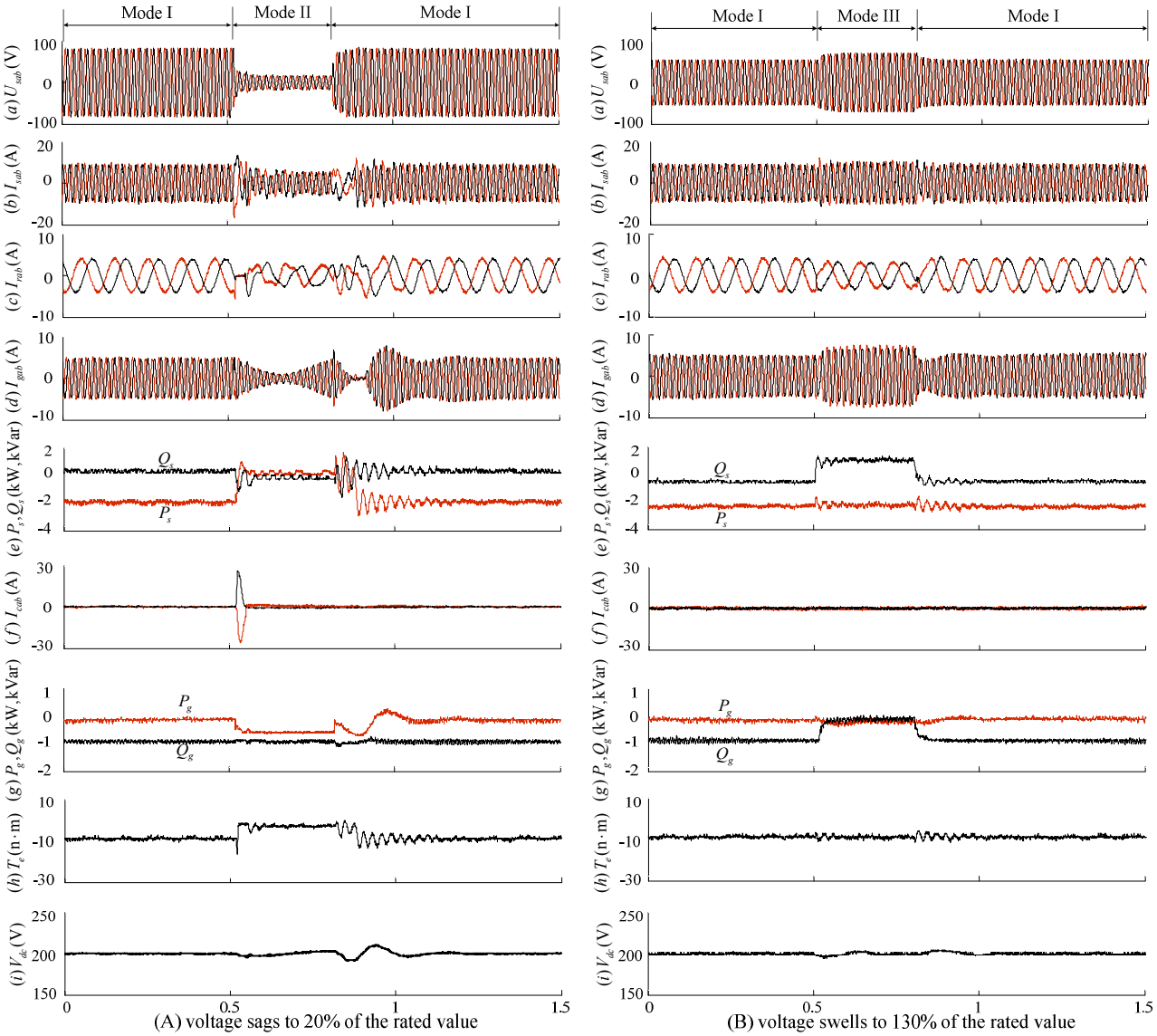

Fig. 11. Experiment results of the DFIG prototype during voltage sag and swell scenarios.

normal operation, i.e., Mode I, are set at $P_s^* = 2k$W and $Q_s^* = 0.5k$ var (inductive), respectively. In addition, the DFIG speed is fixed at 800r/min during the whole test process with the corresponding synchronous speed being 1000r/min. As can be seen from Fig.11 (A), when a grid fault occurs the operation mode of the system is switched immediately from Mode I to Mode II, i.e., once the over-current of the RSC (waveform (i)) is detected, the RSC is deactivated promptly and the crowbar is activated simultaneously (waveform (j)). If the over current is discharged to an acceptable extent by the crowbar device (about 30ms later), the RSC is reactivated with the reactive power supporting (the active power is set to zero) as required, as shown in waveforms (c) and (d). Meanwhile, the GSC is operated in the UPF state since the required reactive current can be entirely provided by the stator of the DFIG, as displayed in waveforms (f) and (g). When the fault is cleared, the system operation mode is then switched from Mode II back to Mode I with the active power gradually controlled up to its normal value. Since the dc-link capacitor used in the tested set-up is a little larger than it needs to be, the oscillations in the dc-bus voltage are not so obvious (waveform (b)) as predicted by the simulation. Fig. 11 (B) shows the high voltage ride-through process of the DFIG system. Compared to Fig. 11 (A), the required reactive current is injected simultaneously from both the stator-side and the GSC of the system, while the output active power is kept the same as its normal value. Nevertheless, the feasibility and effectiveness of the proposed control scheme have been well validated by the experiment results.

Further tests were carried out under different voltage sag and swell cases. The measured waveforms behaved similar to those shown in Fig. 11. However, they are not provided here

due to space limitation.

VI. CONCLUSIONS

In order to meet the latest grid code, a reactive current assignment and control strategy, with its feasibility and effectiveness validated by simulation and experiment results, is proposed to enhance the FRT capability of WTs. As a result, some valuable conclusions can be summarized as follows.

1) In addition to uninterrupted operation, reactive power support during voltage disturbances is another stringent and important regulation in the latest grid codes. To put forward a control scheme capable of meeting the extended regulations, it is necessary to evaluate the reactive power support capability of a DFIG system during grid voltage dips and swells. During grid voltage sag events, the reactive current can be provided mainly or even entirely by the stator-side of the DFIG system. However, in the voltage swell case, the required reactive current should be injected from both the grid- and stator-sides of the system, with the former in priority.
2) The proposed control scheme is implemented with a very simple structure that can be easily and completely transplanted to the existing LVRT application of installed DFIG-based WTs. No extra protection devices are needed in the proposed control but a low-cost crowbar and a chopper, which are usually contained in WTs for LVRT operation. This feature offers the possibility of forming a comprehensive FRT scheme for handling the grid faults of voltage revulsion.
3) Due to limited bandwidth, the traditional PI controller is not able to achieve an effective response to the ac components in current control-loops during voltage sags and swells, which leads to destructive pulsations in the electromagnetic torque if no proper control design is adopted. To simultaneously regulate both the dc and ac components, a compound of a PI regulator plus a resonant controller (PI-R) is introduced with the auxiliary current references calculated. This has been shown to be capable of achieving a more smooth operation. In addition, pitch angle control usually needs to be carefully designed to restrain surges in a turbine's speed under such grid faults, especially during serious voltage sag conditions.

ACKNOWLEDGMENT

The authors want to thank the Natural Science Foundation of Zhejiang Province, China for the financial support (Project No. Y13E070001).

APPENDIX

TABLE I
PARAMETERS OF THE SMULATED DFIG

Rated power	3 MW
Stator voltage/frequency	690 V/50Hz
Stator/rotor turns ratio	0.35
R_s	0.013 p.u.
R_r	0.024 p.u.(referred to the stator)
$L_{\sigma s}$	0.239 p.u.
$L_{\sigma r}$	0.213 p.u. (referred to the stator)
L_m	3.99 p.u.
L_g	0.3 p.u.
R_g	0.01 p.u.
$R_{Crowbar}$	1.6 Ω
$R_{Chopperr}$	2.5 Ω
Lumped inertia const	6.3 s

TABLE II
PARAMETERS OF THE TESTED DFIG

Rated power	5.5 KW
Stator voltage/frequency	380 V/50Hz
Stator/rotor turns ratio	0.33
R_s	1.01 Ω
R_r	0.88 Ω (referred to the stator)
$L_{\sigma s}$	0.0056 H
$L_{\sigma r}$	0.0056 H (referred to the stator)
L_m	0.0875 H
L_g	0.0035H
R_g	0.5 Ω
$R_{Crowbar}$	5 Ω
$R_{Chopperr}$	10 Ω
Lumped inertia const	1.58s

REFERENCES

[1] H. Li and Z. Chen, "Overview of different wind generator systems and their comparisons," *IET Renew Power Generation*, Vol. 2, No. 2, pp. 123-138, Jun. 2008.
[2] R. Cárdenas, R. Peña, S. Alepuz, and G. Asher, "Overview of control systems for the operation of DFIGs in wind energy applications," *IEEE Trans. Ind. Electron*., Vol. 60, No. 7, pp. 2776-2798, Jul. 2013.
[3] M. Mohseni and S. M. Islam, "Review of international grid codes for wind power integration: diversity, technology and a case for global standard," *Renewable and Sustainable Energy Reviews*, Vol. 16, No. 6, pp. 3876-3890, Apr. 2012.
[4] J. Lopez, P. Sanchis, X. Roboam, and L. Marroyo, "Dynamic behavior of the doubly fed induction generator during three-phase voltage dips," *IEEE Trans. Energy Convers.*, Vol. 22, No. 3, pp. 709-717, Sep. 2007.
[5] M. Bongiorno and T. Thiringer, "A generic DFIG model for voltage dip ride-through analysis," *IEEE Trans. Energy Convers*., Vol. 28, No. 1, pp. 76-85, Mar. 2013.
[6] A. Luna, F. K. de Araujo Lima, D. Santos, P. Rodriguez, E. H. Watanabe, and S. Arnaltes, "Simplified modeling of a DFIG for transient studies in wind power applications," *IEEE Trans. Ind. Electron*., Vol. 58, No. 1, pp. 9-20, Jan. 2011.

[7] V. F. Mendes, C. V. de Sousa, and S. R. Silva, "Modeling and ride-through control of doubly fed induction generators during symmetrical voltage sags," *IEEE Trans. Energy Convers*., Vol. 26, No. 4, pp. 1161-1171, Dec. 2011.
[8] D. Xiang, L. Ran, P. J. Tavner, and S. Yang, "Control of doubly fed induction generator in a wind turbine during grid fault ride-through," *IEEE Trans. Energy Convers*., Vol. 21, No. 3, pp. 652-662, Aug. 2006.
[9] J. López, E. Gubía, E. Olea, J. Ruiz, and L. Marroyo, "Ride through of wind turbines with doubly fed induction generator under symmetrical voltage dips," *IEEE Trans. Ind. Electron*., Vol. 56, No. 10, pp. 4246-4254, Oct. 2009.
[10] O. Abdel-Baqi and A. Nasiri, "A dynamic LVRT solution for doubly fed induction generators," *IEEE Trans. Power Electron*., Vol. 25, No. 1, pp. 193-196, Jan. 2010.
[11] G. Pannell, D. J. Atkinson and B. Zahawi, "Minimum-threshold crowbar for a fault-ride-through grid-code-compliant DFIG wind turbine," *IEEE Trans. Energy Convers*., Vol. 25, No. 3, pp. 750-759, Sep. 2010.
[12] J. Yang, J. E. Fletcher, and J. O'Reilly, "A series-dynamic-resistor-based converter protection scheme for doubly-fed induction generator during various fault conditions," *IEEE Trans. Energy Convers*., Vol. 25, No. 2, pp. 422-432, May 2010.
[13] K. E. Okedu, S. M. Muyeen, R. Takahashi, and J. Tamura, "Wind farms fault ride through using DFIG with new protection scheme," *IEEE Trans. Sustain. Energy*, Vol. 3, No. 2, pp. 242-254, Apr. 2012.
[14] M. J. Hossain, T. K. Saha, N. Mithulananthan, and H. R. Pota, "Control strategies for augmenting LVRT capability of DFIGs in interconnected power systems," *IEEE Trans. Ind. Electron*., Vol. 60, No. 6, pp. 2510-2522, Feb. 2013.
[15] L. Wang and D.-N. Truong, "Stability enhancement of DFIG-based offshore wind farm fed to a multi-machine system using a STATCOM," *IEEE Trans. Power Syst*., Vol. 28, No. 3, pp. 2882-2889, Aug. 2013.
[16] M. Mohammadi, M. Gitizadeh, and A. Roosta, "Dynamic stability improvement of a power system incorporating DFIG wind power plant using optimized control parameters of a SVC," in *Proc. IEEE PEDCO*, pp. 416-421, 2012.
[17] A. O. Ibrahim, T. Nguyen, and D. Lee, "A fault ride-through technique of DFIG wind turbine systems using dynamic voltage restorers," *IEEE Trans. Energy Convers*., Vol. 26, No. 3, pp. 871-882, Sep. 2011.
[18] Y. He and J. Hu, "Several hot-spot Issues associated with the grid-connected operations of wind-turbine driven Doubly Fed Induction Generators," in *Proc. CSEE*, Vol. 32, No. 27, pp. 1-15, 2012. (in Chinese)
[19] H. Xu, W. Zhang, and Y. he, "Improved vector control of DFIG based wind turbine during grid dips and swells," in *Proc. IEEE ICEMS*, pp. 511-515, 2010.
[20] M. Mohseni and S. M. Islam, "Transient control of DFIG-based wind power plants in compliance with the Australian Grid Code," *IEEE Trans. Power Electron*., Vol. 27, No.6, pp. 2813-2824, Jun. 2012.
[21] M. Mohseni, M. A. S. Masoum, and S. M. Islam, "Low and high voltage ride-through of DFIG wind turbines using hybrid current controlled converters," *Electrical Power System Research*, Vol. 81, No.7, pp. 1456-1465, Jul. 2011.
[22] C. Wessels and F. W. Fuchs, "High voltage ride through with FACTS for DFIG based wind turbines," in *Proc. Power Electron. App.*, pp.1-10, 2009.
[23] M. N. Eskander and S. I. Amer, "Mitigation of voltage dips and swells in grid-connected wind energy conversion systems," in *Proc. ICCAS-SICE*, pp. 885-890, 2009.
[24] M. Mohseni, S. M. Islam, and M. A. S. Masoum, "Impacts of symmetrical and asymmetrical voltage sags on DFIG-based wind turbines considering phase-angle jump, voltage recovery, and sag parameters," *IEEE Trans. Power Electron*., Vol. 26, No. 5, pp. 1587-1598, May 2011.
[25] H. Xu, W. Zhang, J. Chen, D. Sun, and Y. He, "A high-voltage ride-through control strategy for DFIG based wind turbines considering dynamic reactive power support," in P*roc. the CSEE,* Vol. 33, No. 36, pp. 112-119, 2013. (in chinese)
[26] J. Hu, Y. He, L. Xu, and B. W. Williams, "Improved control of DFIG systems during network unbalance using PI-R current regulators," *IEEE Trans. Ind. Electron*., Vol. 56, No. 2, pp. 439-451, Feb. 2009.
[27] H. Xu, J. Hu, and Y. He, "Integrated modeling and enhanced Control of DFIG under unbalanced and distorted grid voltage conditions," *IEEE Trans. Energy Convers*., Vol. 27, No. 3, pp. 725-736, Sep. 2012.
[28] J. Miret, M. Castilla, J. Matas, J. M. Guerrero, and J. C. Vasquez, "Selective harmonic-compensation control for single-phase active power filter with high harmonic rejection," *IEEE Trans. Ind. Electron*., Vol. 56, No. 8, pp. 3117-3127, Aug. 2009.
[29] Y. Zou, M. Elbuluk, and Y. Sozer, "Stability analysis of maximum power point tracking (MPPT) method in wind power systems," *IEEE Trans. Ind. Appl*., Vol. 49, No. 3, pp. 1129-1136, May/Jun. 2013.

Hailiang Xu was born in China, in 1985. He received his B.S. degree in Electrical Engineering from China University of Petroleum, Dongying, China, in 2008, and his Ph.D. degree in Electrical Engineering from Zhejiang University, Hangzhou, China, in 2014. He has been an postdoctorate student with Academy of Armored Force Engineering, Bejing, China, since 2014. His current research interests include wind power generation systems and electric vehicle drives .

Xiaojun Ma was born in China, in 1963. He received his B.S. degree from Shenyang University of Industry in Industrial Automation, Shenyang, China, in 1985, his M.S. degree from Academy of Armored Force Engineering in Electrical Engineering, Beijing, China, in 1988, and his Ph.D. degree from Tsinghua University in Power System and Automation, Beijing , China, in 1998. In 1988, he joined the Department of Control Engineering, Academy of Armored Force Engineering, where he has been a Professor, since 2000. His current research interests include vehicle electric drive technology and weapon system motion control.

Dan Sun was born in China, in 1971. She received her B.S. degree from Shenyang Jianzhu University, Shenyang, China, in 1997, her M.S. degree from Hehai University, Nanjing, China, in 2000, and her Ph.D. degree from Zhejiang University, Hangzhou, China, in 2004, all in Electrical Engineering. In 2004, she joined the College of Electrical Engineering, Zhejiang University, where she has been an Associate Professor, since 2007. From 2002 to 2004, she was a Visiting Researcher in the University of Technology, Sydney, Australia. From 2009 to 2011, she was a Visiting Professor in the University of Wisconsin, Madison, WI, USA. Her current research interests include advanced electric machine drives and control for wind power generation systems.